J|A|C|S ARTICLES

Published on Web 10/13/2010

Controlling Electron Transfer in Donor−Bridge−Acceptor Molecules Using Cross-Conjugated Bridges

Annie Butler Ricks, Gemma C. Solomon, Michael T. Colvin, Amy M. Scott, Kun Chen, Mark A. Ratner,* and Michael R. Wasielewski*

Department of Chemistry and Argonne-Northwestern Solar Energy Research (ANSER) Center, Northwestern University, Evanston, Illinois 60208-3113, United States

Received August 17, 2010; E-mail: m-wasielewski@northwestern.edu

Abstract: Photoinitiated charge separation (CS) and recombination (CR) in a series of donor−bridge−acceptor (D−B−A) molecules with cross-conjugated, linearly conjugated, and saturated bridges have been compared and contrasted using time-resolved spectroscopy. The photoexcited charge transfer state of 3,5-dimethyl-4-(9-anthracenyl)julolidine (DMJ−An) is the donor, and naphthalene-1,8:4,5-bis(dicarboximide) (NI) is the acceptor in all cases, along with 1,1-diphenylethene, *trans*-stilbene, diphenylmethane, and xanthone bridges. Photoinitiated CS through the cross-conjugated 1,1-diphenylethene bridge is about 30 times slower than through its linearly conjugated *trans*-stilbene counterpart and is comparable to that observed through the diphenylmethane bridge. This result implies that cross-conjugation strongly decreases the π orbital contribution to the donor−acceptor electronic coupling so that electron transfer most likely uses the bridge σ system as its primary CS pathway. In contrast, the CS rate through the cross-conjugated xanthone bridge is comparable to that observed through the linearly conjugated *trans*-stilbene bridge. Molecular conductance calculations on these bridges show that cross-conjugation results in quantum interference effects that greatly alter the through-bridge donor−acceptor electronic coupling as a function of charge injection energy. These calculations display trends that agree well with the observed trends in the electron transfer rates.

Introduction

The ability to promote and control charge transport over long distances is essential to the development of solar energy conversion systems and molecule-based electronics.[1−6] Photoinitiated multistep electron transfer in photosynthetic reaction center proteins, where charge is transferred across about 4 nm with near unity efficiency, is an important model for designing molecular donor−bridge−acceptor (D−B−A) systems to achieve efficient, long-lived, long-distance charge separation.[7,8] The electron transfer characteristics of D−B−A systems are usually determined by time-resolved spectroscopic measurements of photoinitiated charge separation (CS) leading to $D^{+\bullet}-B-A^{-\bullet}$ radical ion pairs (RPs) that subsequently undergo dark charge recombination (CR). In comparison, studies of charge transport in wire-like molecules for molecular electronics often focus on the dark conductance of bridge molecules that link two metallic contacts.[9,10] In a formal sense, the two approaches are related in that the D and A molecules in the D−B−A systems serve a similar role as that of the metallic contacts in the conductance measurements.

D−B−A systems provide a means of systematically studying electron transfer through bridge molecules such as DNA base pairs,[11−13] peptides in proteins,[14] porphyrins,[15,16] saturated alkane σ-systems,[17,18] and unsaturated π-conjugated alkene, alkyne, and aromatic spacers.[19−27] In order to design D−B−A systems with predictable electron transfer properties, it is

(1) Jortner, J.; Ratner, M. A. *Molecular Electronics*; Blackwell: London, 1997.
(2) Gust, D.; Moore, T. A.; Moore, A. L. *Chem Commun (Cambridge, U.K.)* **2006**, 1169–1178.
(3) Nijhuis, C. A.; Reus, W. F.; Whitesides, G. M. *J. Am. Chem. Soc.* **2009**, *131*, 17814–17827.
(4) Lukas, A. S.; Miller, S. E.; Wasielewski, M. R. *J. Phys. Chem. B* **2000**, *104*, 931–940.
(5) Mujica, V.; Ratner, M. A.; Nitzan, A. *Chem. Phys.* **2002**, *281*, 147–150.
(6) Winters, M. U.; Dahlstedt, E.; Blades, H. E.; Wilson, C. J.; Frampton, M. J.; Anderson, H. L.; Albinsson, B. *J. Am. Chem. Soc.* **2007**, *129*, 4291–4297.
(7) Wasielewski, M. R. *Chem. Rev.* **1992**, *92*, 435–461.
(8) Parson, W. W. *Science* **2007**, *316*, 1438–1439.
(9) Wang, C. S.; Batsanov, A. S.; Bryce, M. R.; Martin, S.; Nichols, R. J.; Higgins, S. J.; Garcia-Suarez, V. M.; Lambert, C. J. *J. Am. Chem. Soc.* **2009**, *131*, 15647–15654.
(10) Fan, F. R. F.; Yang, J. P.; Cai, L. T.; Price, D. W.; Dirk, S. M.; Kosynkin, D. V.; Yao, Y. X.; Rawlett, A. M.; Tour, J. M.; Bard, A. J. *J. Am. Chem. Soc.* **2002**, *124*, 5550–5560.
(11) Jortner, J.; Bixon, M.; Langenbacher, T.; Michel-Beyerle, M. E. *Proc. Natl. Acad. Sci. U.S.A.* **1998**, *95*, 12759–12765.
(12) Lewis, F. D.; Wu, T.; Zhang, Y.; Letsinger, R. L.; Greenfield, S. R.; Wasielewski, M. R. *Science* **1997**, *277*, 673–676.
(13) Daublain, P.; Siegmund, K.; Hariharan, M.; Vura-Weis, J.; Wasielewski, M. R.; Lewis, F. D.; Shafirovich, V.; Wang, Q.; Raytchev, M.; Fiebig, T. *Photochem. Photobiol. Sci.* **2008**, *7*, 1501–1508.
(14) Gray, H. B.; Winkler, J. R. *Proc. Natl. Acad. Sci. U.S.A.* **2005**, *102*, 3534–3539.
(15) Winters, M. U.; Karnbratt, J.; Blades, H. E.; Wilson, C. J.; Frampton, M. J.; Anderson, H. L.; Albinsson, B. *Chem.—Eur. J.* **2007**, *13*, 7385–7394.
(16) Kobori, Y.; Yamauchi, S.; Akiyama, K.; Tero-Kubota, S.; Imahori, H.; Fukuzumi, S.; Norris, J. R., Jr. *Proc. Natl. Acad. Sci. U.S.A.* **2005**, *102*, 10017–10022.
(17) Hush, N. S.; Paddon-Row, M. N.; Cotsaris, E.; Oevering, H.; Verhoeven, J. W.; Heppener, M. *Chem. Phys. Lett.* **1985**, *117*, 8–11.
(18) Paulson, B. P.; Miller, J. R.; Gan, W. X.; Closs, G. *J. Am. Chem. Soc.* **2005**, *127*, 4860–4868.

essential to understand how the electronic structure and composition of the bridge plays a role in governing the rates of electron transfer. Electron transfer in D−B−A systems occurs most often by a superexchange mechanism involving virtual bridge states.[19,28−31] Qualitatively, the superexchange mechanism results in three observed trends in electron transfer rates: (1) increasing bridge length decreases the rate; (2) charge transport through a fully conjugated bridge is faster than through a saturated bridge; (3) a larger energy gap between the starting state of the charge transfer process and the relevant virtual bridge states leads to decreased electron transfer rates.[32]

In more quantitative terms, through-bond electron transfer rate constants most often decay exponentially with donor−acceptor distance as described by eq 1

$$k = k_0 e^{-\beta(r-r_0)} \tag{1}$$

where k_0 is the rate constant at the van der Waals contact distance r_0 (3.5 Å), and β is an exponential damping factor. This behavior is characteristic of the superexchange mechanism in which the β values depend on both the electronic coupling matrix element for the charge transfer process, V_{DA}, as well as the energy gap for charge injection from the donor to the virtual bridge state, ΔE_{DB},[28,29]

$$V_{DA} = \frac{V_{DB}V_{BA}}{\Delta E_{DB}}\left(\frac{V_{BB}}{\Delta E_{DB}}\right)^{N-1} \tag{2}$$

where β is described by

$$\beta = \frac{2}{r}\ln\left(\frac{\Delta E_{DB}}{V_{BB}}\right) \tag{3}$$

and where V_{DB} and V_{BA} are the matrix elements that couple the donor to the bridge and the bridge to the acceptor, respectively, V_{BB} is the electronic coupling between bridge sites, N is the number of identical bridge sites, and r is the length of one bridge segment. Equation 2 is approximate and does not take into account non-nearest neighbor interactions and multiple pathways.[33] The β value is affected by bridge length[34,35] and conformational rigidity,[36] as well as the electronic properties of the donor and acceptor.[22,36]

Recently, theory has predicted that certain molecules will have quantum interference effects that will strongly influence electron transfer rates. Cross-conjugated molecules are one such class of compounds where it is thought that these interference effects will be large.[32] Cross-conjugation is defined as "a compound possessing three unsaturated groups, two of which although conjugated to a third unsaturated center are not conjugated to each other. The word conjugated is defined here in the classical sense of denoting a system of alternating single and double bonds."[37] Although the term cross-conjugation is used infrequently, molecules that exhibit this particular type of conjugation are common in chemistry, e.g., quinones, radialenes, fulvalenes, and various fused aromatics.[38] The effects of cross-conjugation on charge transfer states in molecular systems have been examined with a view toward nonlinear optical materials,[39,40] magnetic materials,[41,42] as well as donor−acceptor interactions.[23,43,44] In addition, many oligomers and polymers with cross-conjugated frameworks have recently been synthesized for advanced materials.[38,45,46]

Theoretical work has examined the relationship between charge transfer and charge transport[47] in D−B−A molecules in which D and A are attached to metallic contacts. This work has shown that it is possible to separate the contributions from the metallic contacts in molecular conductance measurements from the intrinsic charge transfer rates from D to A, revealing the underlying commonality: the electronic coupling through the bridge. In this way, it can be shown that molecular conductance is approximately proportional to the electron transfer rate, with the contributions from the metallic contacts and the donor and acceptor scaling the result and preventing a direct equality.

$$g \approx \frac{8e^2}{\pi^2\Gamma_D^{(L)}\Gamma_D^{(R)}F}\,k_{D\to A} \tag{4}$$

Here g is the conductance, e is the charge on an electron, Γ is the influence of the leads in perturbing the bridging molecule,

(19) Albinsson, B.; Eng, M. P.; Pettersson, K.; Winters, M. U. *Phys. Chem. Chem. Phys.* **2007**, *9*, 5847–5864.
(20) Albinsson, B.; Martensson, J. *J. Photochem. Photobiol., C* **2008**, *9*, 138–155.
(21) Weiss, E. A.; Ahrens, M. J.; Sinks, L. E.; Gusev, A. V.; Ratner, M. A.; Wasielewski, M. R. *J. Am. Chem. Soc.* **2004**, *126*, 5577–5584.
(22) Goldsmith, R. H.; Sinks, L. E.; Kelley, R. F.; Betzen, L. J.; Liu, W.; Weiss, E. A.; Ratner, M. A.; Wasielewski, M. R. *Proc. Natl. Acad. Sci. U.S.A.* **2005**, *102*, 3540–3545.
(23) Molina-Ontoria, A.; Fernandez, G.; Wielopolski, M.; Atienza, C.; Sanchez, L.; Gouloumis, A.; Clark, T.; Martin, N.; Guldi, D. M. *J. Am. Chem. Soc.* **2009**, *131*, 12218–12229.
(24) Lembo, A.; Tagliatesta, P.; Guldi, D. M.; Wielopolski, M.; Nuccetelli, M. *J. Phys. Chem. A* **2009**, *113*, 1779–1793.
(25) Wielopolski, M.; Atienza, C.; Clark, T.; Guldi, D. M.; Martin, N. *Chem.—Eur. J.* **2008**, *14*, 6379–6390.
(26) Martin, N.; Giacalone, F.; Segura, J. L.; Martin, N.; Guldi, D. M. *Synth. Met.* **2004**, *147*, 57–61.
(27) Guldi, D. M.; Luo, C.; Swartz, A.; Gomez, R.; Segura, J. L.; Martin, N. *J. Phys. Chem. A* **2004**, *108*, 455–467.
(28) McConnell, H. M. *J. Chem. Phys.* **1961**, *35*, 508–515.
(29) Ratner, M. A. *J. Phys. Chem.* **1990**, *94*, 4877–4883.
(30) Davis, W. B.; Ratner, M. A.; Wasielewski, M. R. *J. Am. Chem. Soc.* **2001**, *123*, 7877–7886.
(31) Davis, W. B.; Svec, W. A.; Ratner, M. A.; Wasielewski, M. R. *Nature* **1998**, *396*, 60–63.
(32) Solomon, G. C.; Andrews, D. Q.; Van Duyne, R. P.; Ratner, M. A. *J. Am. Chem. Soc.* **2008**, *130*, 7788–7789.
(33) Onuchic, J. N.; Deandrade, P. C. P.; Beratan, D. N. *J. Chem. Phys.* **1991**, *95*, 1131–1138.
(34) Lukas, A. S.; Bushard, P. J.; Weiss, E. A.; Wasielewski, M. R. *J. Am. Chem. Soc.* **2003**, *125*, 3921–3930.
(35) Weiss, E. A.; Ratner, M. A.; Wasielewski, M. R. *J. Phys. Chem. A* **2003**, *107*, 3639–3647.
(36) Weiss, E. A.; Tauber, M. J.; Kelley, R. F.; Ahrens, M. J.; Ratner, M. A.; Wasielewski, M. R. *J. Am. Chem. Soc.* **2005**, *127*, 11842–11850.
(37) Phelan, N. F.; Orchin, M. *J. Chem. Educ.* **1968**, *45*, 633–637.
(38) Gholami, M.; Tykwinski, R. R. *Chem. Rev.* **2006**, *106*, 4997–5027.
(39) Wang, H.; Helgeson, R.; Ma, B.; Wudl, F. *J. Org. Chem.* **2000**, *65*, 5862–5867.
(40) Lee, S.; Thomas, K. R. J.; Thayumanavan, S.; Bardeen, C. J. *J. Phys. Chem. A* **2005**, *109*, 9767–9774.
(41) Shultz, D. A.; Fico, R. M., Jr.; Bodnar, S. H.; Kumar, R. K.; Vostrikova, K. E.; Kampf, J. W.; Boyle, P. D. *J. Am. Chem. Soc.* **2003**, *125*, 11761–11771.
(42) Sandberg, M. O.; Nagao, O.; Wu, Z.; Matsushita, M. M.; Sugawara, T. *Chem. Commun. (Cambridge, U.K.)* **2008**, 3738–3740.
(43) Thompson, A. L.; Ahn, T.-S.; Thomas, K. R. J.; Thayumanavan, S.; Martinez, T. J.; Bardeen, C. J. *J. Am. Chem. Soc.* **2005**, *127*, 16348–16349.
(44) Gonzalez-Rodriguez, D.; Torres, T.; Herranz, M. A.; Echegoyen, L.; Carbonell, E.; Guldi, D. M. *Chem.—Eur. J.* **2008**, *14*, 7670–7679.
(45) Ortiz, R. P.; Facchetti, A.; Marks, T. J.; Casado, J.; Zgierski, M. Z. *Adv. Funct. Mater.* **2009**, *19*, 386–394.
(46) Li, H. R.; Valiyaveettil, S. *Macromolecules* **2007**, *40*, 6057–6066.
(47) Nitzan, A. *J. Phys. Chem. A* **2001**, *105*, 2677–2679.

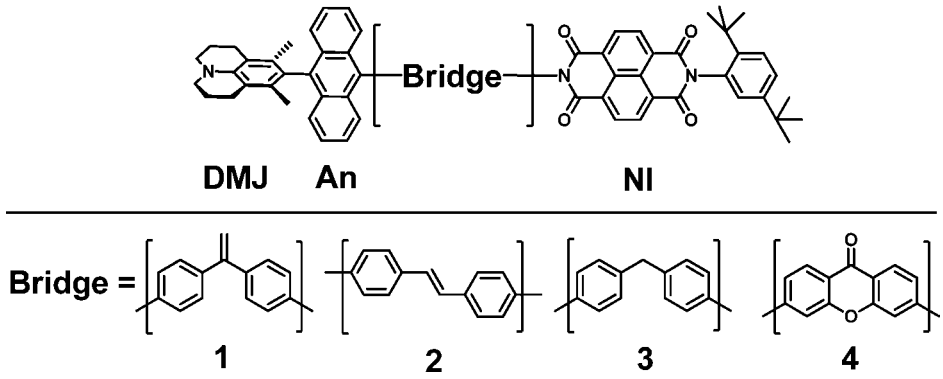

Figure 1. Chemical structures of the molecules used in this study.

F is the thermally averaged Franck−Condon weighted density of nuclear states of the donor and acceptor, and $k_{D\rightarrow A}$ is the rate. This result leads to the supposition that there may be circumstances where a ratio of charge transfer rates shows the same trends as ratios of conductance or charge transport. The extent to which such a relationship will quantitatively hold is limited by a number of factors. Equation 4 is derived under a number of assumptions that should be noted at this point. First, this relationship was derived for the case in which the full D−B−A system is bound between metallic electrodes, rather than binding a bridge directly to electrodes as is more common in molecular electronics experiments. Second, the relationship is derived with the assumption that coherent tunneling (superexchange) dominates both electron transfer and transport. Finally, although not an assumption of the derivation, for a comparison between the different bridges to hold, the influence of the electrodes and the donor and acceptor must be equal in both cases to ensure that the prefactors cancel. Comparing electron transport theory with electron transfer experiments seems unlikely to yield a quantitative comparison. However, the relationship in eq 4 provides a basis for a qualitative comparison, and we expect to see the trends observed in the electron transfer rates through the series of bridges reflected in the trends for electron transport.

In this study, we report the results of our investigation into photoinduced electron transfer in a D−B−A system where different bridges are used to probe the effects of cross-conjugation on CS and CR rates. These rates are compared with the predictions of molecular conductance calculations for the same bridges. The 3,5-dimethyl-4-(9-anthracenyl)julolidine (DMJ−An) donor and the naphthalene-1,8:4,5-bis(dicarboximide) (NI) acceptor are linked using one of four different bridges (Figure 1). In molecule **1**, the 1,1-diphenylethene bridge is cross-conjugated, since both phenyls are linearly conjugated to the double bond, but not to each other. In molecule **2**, the *trans*-stilbene bridge is linearly conjugated,[48] while in **3**, the diphenylmethane bridge possesses a saturated CH_2 group that breaks the direct conjugated pathway between the phenyls. In molecule **4**, the xanthone bridge is also cross-conjugated, since both phenyls are linearly conjugated to the ketone, but not to each other. The xanthone bridge tests how substituent effects, as represented by the oxygen atom of the carbonyl group, alter charge transport through a cross-conjugated bridge.

The trends predicted by the molecular conductance calculations are clearly reflected in the observed CS and CR rates. Although a metallic electrode is chemically distinct from molecular donor and acceptor components, the results show that there is significant common ground between the two contexts.

Experimental Section

Synthesis and Steady-State Spectroscopy. The synthesis and characterization of **1**−**4** are described in the Supporting Information. All reagents were purchased from Sigma-Aldrich and used as received. All final products were purified by normal-phase preparative thin layer chromatography prior to characterization. All solvents were spectrophotometric grade or distilled prior to use. Intermediates and the resulting products were characterized by ^{1}H NMR, HR-MS, and UV−vis spectroscopy.

Steady-state absorption spectroscopy was performed using a Shimadzu (UV-1601) spectrophotometer. All solvents were spectroscopic grade and used as is, except for tetrahydrofuran (THF), which was further purified by passing it twice through alumina (GlassContour) immediately prior to use.

Energy Levels and Molecular Structures. Given that photoexcitation of DMJ−An results in quantitative subpicosecond charge separation to produce $DMJ^{+\bullet}-An^{-\bullet}$ with a spectroscopically determined energy of 2.89 eV in toluene,[49] the energy levels for the charge separated states, $DMJ^{+\bullet}-An-B-NI^{-\bullet}$, $DMJ-An-B^{+\bullet}-NI^{-\bullet}$, and $DMJ^{+\bullet}-An-B^{-\bullet}-NI$ were determined in toluene using eq 5

$$\Delta G_F = \Delta G_I + \mathrm{sign}(E_I - E_F) + \frac{e^2}{\varepsilon_s}\left(\frac{1}{r_1} - \frac{1}{r_F}\right) \qquad (5)$$

where ΔG_I and ΔG_F are the energies above ground state for the initial and final ion pairs, respectively, E_I and E_F are the redox potentials for the initial and final ions, respectively, between which the electron is transferred, r_I and r_F are the initial and final ion pair distances, respectively, e is the electronic charge, and ε_s is the static dielectric constant of the solvent ($\varepsilon_s = 2.38$ for toluene), and the sign = (−) if $E_F > E_I$ and the sign = (+) if $E_I > E_F$. The distances r_I and r_F between the donor, bridge, and acceptor components were determined from the energy-minimized structures of DMJ−An−B−NI determined with density functional theory (DFT) using Becke's[50] three-parameter hybrid functional with Lee, Yang, and Parr[51] correction functional (B3LYP) and the STO-3G basis set. The redox potentials of DMJ, An, the bridges, and NI are given in the Supporting Information, and the ion pair distances and energies are listed in Table S1 and illustrated in Figure S1 of the Supporting Information.

(48) Van Walree, C. A.; Kaats-Richters, V. E. M.; Veen, S. J.; Wieczorek, B.; Van Der Wiel, J. H.; Van Der Wiel, B. C. *Eur. J. Org. Chem.* **2004**, 3046–3056.

(49) Dance, Z. E. X.; Ahrens, M. J.; Vega, A. M.; Ricks, A. B.; McCamant, D. W.; Ratner, M. A.; Wasielewski, M. R. *J. Am. Chem. Soc.* **2008**, *130*, 830–832.

(50) Becke, A. D. *J. Chem. Phys.* **1993**, *98*, 1372–1377.

(51) Lee, C.; Yang, W.; Parr, R. G. *Phys. Rev. B* **1988**, *37*, 785–789.

Transient Absorption Spectroscopy. Femtosecond transient absorption measurements were made using the 416-nm frequency-doubled output from a regeneratively amplified titanium:sapphire laser system operating at 2 kHz.[21] A white light continuum probe pulse was generated by focusing the IR fundamental into a 1-mm sapphire disk.[52] Detection with a CCD spectrograph has previously been described.[52] The optical density of all samples was maintained between 0.3 and 0.5 at 416 nm, and the samples were placed in a 2 mm path length quartz cuvette equipped with a vacuum adapter and subjected to five freeze−pump−thaw degassing cycles prior to transient absorption measurements. The samples were irradiated with 1.0 μJ per pulse focused to a 200 μm spot. Typically, 5 to 7 s of averaging was used to obtain the transient spectrum at a given delay time. The total instrument response function (IRF) for the pump−probe experiments was 180 fs. Transient absorption kinetics were determined at a given wavelength by using a nonlinear least-squares fit to a general sum of exponentials, using the Levenberg−Marquardt algorithm, while accounting for the presence of the finite instrument response.

Samples for nanosecond transient absorption spectroscopy were placed in a 10 mm path length quartz cuvette and freeze−pump−thawed five times. The samples were excited with 7 ns, 2.5 mJ, 416 nm using the frequency-tripled output of a Continuum Precision II 8000 Nd:YAG laser to pump a Continuum Panther OPO. The excitation pulse was directed to a 5 mm diameter spot and matched to the diameter of the probe pulse generated using a xenon flashlamp (EG&G Electro-Optics FX-200). Kinetic traces were detected from 430−800 nm every 5 nm using a monochromator and photomultiplier tube with high voltage applied to only four dynodes (Hamamatsu R928). The total instrument response time is 7 ns and is determined primarily by the laser pulse duration. Analysis of the kinetic data was performed at multiple wavelengths using a Levenberg−Marquardt nonlinear least-squares fit to a general sum-of-exponentials function with an added Gaussian function to account for the finite instrument response.

For the magnetic field effect experiments, the sample cuvette was placed between the poles of a Walker Scientific HV-4W electromagnet powered by a Walker Magnion HS-735 power supply, and the field strength was measured by a Lakeshore gaussmeter with a Hall effect probe. The electromagnet and gaussmeter were interfaced with Labview, allowing measurements and control of the magnetic field to $\pm 1 \times 10^{-5}$ T during the data acquisition. To maintain sample integrity during the experiment, a probe light shutter was used to block the sample from irradiation when transient absorption kinetics were not being collected. The triplet yield was monitored at 480 and 430 nm and kinetic traces were collected in increments of 0.3, 1.5, or 5.0 mT with zero field $\Delta A(B = 0)$ collection after four or five steps. To compensate for possible sample degradation, zero field kinetics were collected during the experiment in four- or five-step increments and plotted and fit with polynomial or linear trend lines. These functions were used to calculate the relative RP yield or triplet yield as a function of applied field strength (B) and plotted as $\Delta A(B)/\Delta A(B = 0)$. The results presented are an average of three or more experiments conducted on separate days with freshly prepared samples in spectrophotometric or freshly distilled ACS-grade toluene.

Time-Resolved EPR Measurements. Toluene solutions of **1**, **3**, and **4** ($\sim 10^{-4}$ M) were loaded into quartz tubes (4 mm o.d. × 2 mm i.d.), subjected to five freeze−pump−thaw degassing cycles on a vacuum line (10^{-4} mBar), and sealed using a hydrogen torch. Time-resolved EPR (TREPR) measurements were made at X-band using continuous wave (CW) microwaves and direct detection on a Bruker E-580 spectrometer. Sample temperatures were controlled by an Oxford Instruments CF935 cryostat using liquid N_2. Samples were photoexcited at 416 nm using the output from a frequency-tripled, H_2-Raman shifted Nd:YAG laser (1−2 mJ/pulse, 7 ns, 10 Hz, QuantaRay Lab-150). The polarization of the laser was set to 54.7° relative to the direction of the static magnetic field to avoid magnetophotoselection effects on the spectra. Following photoexcitation, kinetic traces of the transient magnetization were accumulated under CW microwave irradiation (6−20 mW). The field modulation was disabled to achieve a $Q/\pi\nu \approx 30$ ns instrument response function (IRF), where Q is the quality factor of the resonator and ν is the resonant frequency, while microwave signals in emission (e) and/or enhanced absorption (a) were detected in both the real and the imaginary channels (quadrature detection). Sweeping the magnetic field gave 2D spectra versus both time and magnetic field. For each kinetic trace, the signal acquired prior to the laser pulse was subtracted from the data. Kinetic traces recorded at magnetic field values off-resonance were considered background signals, whose average was subtracted from all kinetic traces. The spectra were subsequently phased into a Lorentzian part and a dispersive part, and the former, also known as the imaginary magnetic susceptibility χ", is presented.

Transport Calculations. In the coherent tunneling limit the conductance through a molecule is frequently calculated with what is known as the Landauer approach. At this level the current through a molecule is defined as:

$$I(V) = \frac{2e}{h}\int_{-\infty}^{\infty} \mathrm{d}E\ \mathrm{Tr}[T(E,V)](f_{\mathrm{L}}(E) - f_{\mathrm{R}}(E)) \qquad (6)$$

where e is the charge on an electron, h is Planck's constant, $T(E,V)$ is the transmission through the molecule, and f_{L} and f_{R} are the Fermi functions for the two electrodes. The Fermi functions define the occupation of the electrodes and set the energy window over which transport occurs at a given voltage. The differential conductance is given in eq 7.

$$g(V) = \frac{\mathrm{d}I(V)}{\mathrm{d}V} \qquad (7)$$

As the applied bias approaches zero, the differential conductance can be approximated as the transmission at the (now common) Fermi energy of the two electrodes:

$$g(0) \approx T(E_{\mathrm{F}}) \qquad (8)$$

In order to understand the relationship in eq 4 we assume that the transmission at some unknown energies can be related to the observed rates for charge separation and recombination. Consequently, the electronic transmission will be plotted over a substantial energy range, and the trends across the bridges will be examined for energy windows in which the trends match the observed rates.

All transport calculations were performed for the bridges with thiol groups substituted in the place of the donor and acceptor (designated **1S**, **2S**, **3S**, and **4S**), to allow binding to gold electrodes. Geometries for thiol-substituted bridges were optimized with Qchem3.0[53] using density functional theory with B3LYP and 6-311G**. The thiol hydrogen atoms were removed, and these systems were bound to planar gold electrodes with gold−sulfur distances taken from the literature.[54] The transport calculations were performed using gDFTB.[55−58] In the cases where the dependence

(52) Giaimo, J. M.; Gusev, A. V.; Wasielewski, M. R. *J. Am. Chem. Soc.* **2002**, *124*, 8530–8531.

(53) Shao, Y.; et al. *Phys. Chem. Chem. Phys.* **2006**, *8*, 3172–3191.

(54) Bilic, A.; Reimers, J. R.; Hush, N. S. *J. Chem. Phys.* **2005**, *122*, 094708−094715.

(55) Elstner, M.; Porezag, D.; Jugnickel, G.; Elsner, J.; Haugk, M.; Frauenheim, T.; Suhai, S.; Seifert, G. *Phys. Rev. B* **1998**, *58*, 7260–7268.

(56) Frauenheim, T.; Seifert, G.; Elstner, M.; Hagnal, Z.; Jungnickel, G.; Porezag, D.; Suhai, S.; Scholz, R. *Phys. Status Solidi B* **2000**, *217*, 41–62.

(57) Frauenheim, T.; Seifert, G.; Elstner, M.; Niehaus, T.; Koehler, C.; Amkreutz, M.; Sternberg, M.; Hajnal, Z.; Di Carlo, A.; Suhai, S. *J. Phys.: Condens. Matter* **2002**, *14*, 3015–3047.

(58) Pecchia, A.; Di Carlo, A. *Rep. Prog. Phys.* **2004**, *67*, 1497–1561.

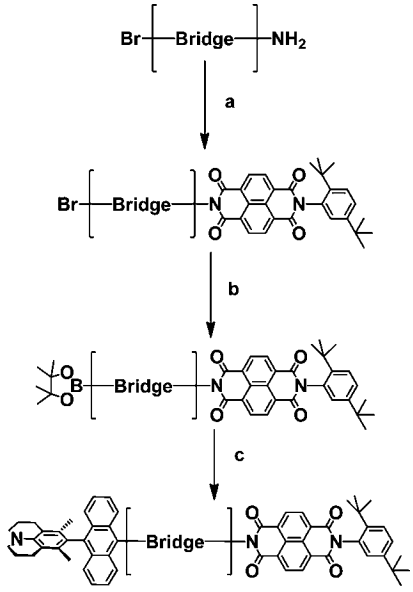

Figure 2. General synthetic scheme for **1**−**4**. (a) *N*-(2,5-di-*tert*-butylphenyl)-naphthalene-1,8-dicarboxyanhydride-4,5-dicarboximide, pyridine reflux; (b) bis(pinacolato)diboron, DMF, KOAc, $PdCl_2(dppf)$, 75 °C; (c) 3,5-dimethyl-4-(10-bromoanthracenyl)julolidine, $Pd_2(dba)_3$, $P(o\text{-}tol)_3$, Ag_2O, THF, 70 °C.

of the transmission on the molecular conformation was investigated, the optimized structures were modified by varying the dihedral as noted, but not reoptimized in each step.

Results

Synthesis and Steady-State Spectroscopy. The syntheses of compounds **1**−**4** are summarized in Figure 2, and the details are given in the Supporting Information. Briefly, the bridges are synthesized with one bromo and one amino substituent at the appropriate positions. Each bridge is then reacted with *N*-(2,5-di-*tert*-butylphenyl)naphthalene-1,8-dicarboxyanhydride-4,5-dicarboximide[59] in pyridine to form Br−bridge−NI. The bromo group is then converted into a boronic ester using bis(pinacolato)diboron and a Pd catalyst in toluene, and the resulting boronic ester is linked to DMJ−An−Br using Pd-catalyzed Suzuki coupling to give compounds **1**−**4**.

The ground-state absorption spectrum of DMJ−An in toluene exhibits a broad CT absorption maximum at 367 nm with a broad emission maximum at 519 nm, resulting in an excited singlet CT state energy of 2.89 eV.[49,60] The ground-state electronic absorption spectra of compounds **1**−**4** (Figure 3) have maxima at 360 nm, 380 nm, and 398 nm, with the prominent vibronic structure resulting from overlapping contributions of the DMJ−An charge transfer (CT) absorption[49] and the NI acceptor Franck−Condon progressions.[4] Additionally, for **2**, there is a broad feature between 300 and 350 nm due to the *trans*-stilbene bridge. The remainder of the bridges absorb primarily to the blue of 300 nm.[48,61,62] As the bridge is changed, no significant changes are observed in the absorption spectrum,

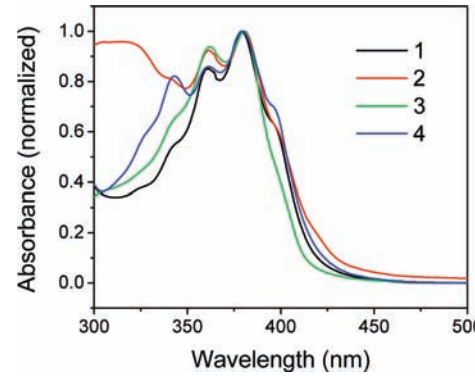

Figure 3. Normalized ground-state absorption spectra of **1**−**4**.

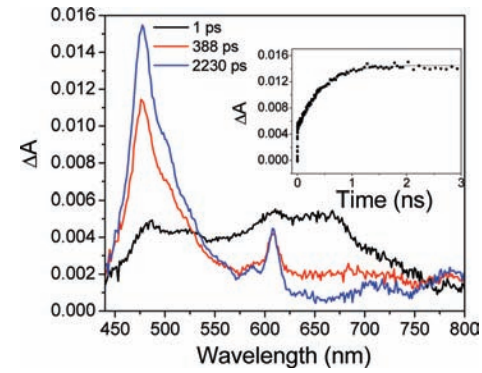

Figure 4. Transient absorption spectra of **1** in toluene at 293 K at the indicated times following excitation. Inset: transient absorption kinetics at 480 nm.

which indicates that in each case the bridge is weakly electronically coupled to the donor and acceptor.

Transient Absorption Spectroscopy. Femtosecond transient absorption measurements were performed in toluene on molecules **1**−**4** using 130-fs, 416-nm pulses to selectively excite the DMJ−An CT state. The transient absorption spectrum for **1** is shown in Figure 4, while the spectra for **2**−**4** are shown in Figure S2, Supporting Information. At early times, the broad absorption features centered at 490 nm ($\varepsilon = 4500\ M^{-1}cm^{-1}$)[63] and 680 nm ($\varepsilon = 10\,000\ M^{-1}cm^{-1}$) are attributed to $DMJ^{+\bullet}$ and $An^{-\bullet}$, respectively. As the final step of the charge separation occurs for **1**−**4**, $DMJ^{+\bullet}-An^{-\bullet}-B-NI \rightarrow DMJ^{+\bullet}-An-B-NI^{-\bullet}$, the formation of prominent absorption bands due to $NI^{-\bullet}$ are distinctly seen at 480 and 610 nm ($\varepsilon_{480} = 25\,500\ M^{-1}cm^{-1}$).[64] No large spectral differences were observed between the molecules in this series, but the charge separation times (τ_{CS}) differ significantly. The rise of $NI^{-\bullet}$ was monitored at 480 nm, giving the τ_{CS} values for **1**−**4** shown in Table 1.

Nanosecond transient absorption measurements were performed in toluene using 7-ns, 416-nm pulses to measure the charge recombination times (τ_{CR}) through the various bridges for molecules **1**−**4**. Formation of the $NI^{-\bullet}$ absorption bands at 480 and 610 nm was again observed, and the values of τ_{CR} were determined at these wavelengths (Figure S3, Supporting Information). The absorption features at later times in the 400 to 500 nm range are attributed to $^{3*}An$, which is generated upon charge recombination. The charge recombination times are listed in Table 1.

(59) Carmieli, R.; Mi, Q.; Butler Ricks, A.; Giacobbe, E. M.; Mickley, S. M.; Wasielewski, M. R. *J. Am. Chem. Soc.* **2009**, *131*, 8372–8373.
(60) Lockard, J. V.; Butler Ricks, A.; Co, D. T.; Wasielewski, M. R. *J. Phys. Chem. Lett.* **2010**, *1*, 215–218.
(61) Garner, A.; Wilkinson, F. *J. Chem. Soc., Faraday Trans. 2* **1976**, *72*, 1010–1020.
(62) Cooke, D. W.; Muenchausen, R. E.; Bennett, B. L.; Wrobleski, D. A.; Orler, E. B. *Radiat. Phys. Chem.* **2003**, *66*, 129–135.
(63) Okada, T.; Fujita, T.; Kubota, M.; Masaki, S.; Mataga, N.; Ide, R.; Sakata, Y.; Misumi, S. *Chem. Phys. Lett.* **1972**, *14*, 563–568.
(64) Gosztola, D.; Niemczyk, M. P.; Svec, W. A.; Lukas, A. S.; Wasielewski, M. R. *J. Phys. Chem. A* **2000**, *104*, 6545–6551.

Table 1. Charge Separation (τ_{CS}) and Recombination Times (τ_{CR}) Measured by Transient Absorption, and the Spin−Spin Exchange Interaction, 2*J*, Measured by MFE and TREPR

compound	τ_{CS} (ps)	τ_{CR} (ns)	2*J* (mT)
1	395 ± 10	1044 ± 36	0.4 ± 0.2[a]
2	14 ± 1	107 ± 5	29.0 ± 1[b]
3	460 ± 6	287 ± 18	2 ± 0.5[a]
4	6 ± 1	155 ± 3	3.5 ± 0.5[a,b]

[a] Measured by TREPR. [b] Measured by MFE.

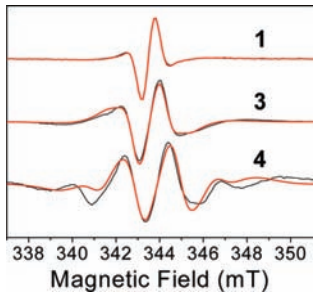

Figure 5. TREPR spectra of **1**, **3**, and **4** in toluene at 295 K, following a 7 ns, 416 nm laser pulse. Simulations are shown in red.

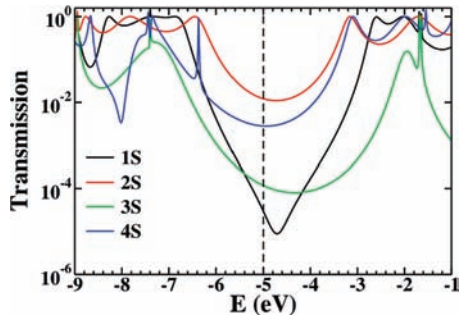

Figure 6. The transmission through the thiol-substituted bridges bound between metallic electrodes. Over a large range the transmission through **1S** and **3S** is significantly lower than that through **2S** and **4S**.

Time-Resolved EPR Measurements. We employed TREPR to obtain the spin−spin exchange interaction (2*J*) in the photogenerated RPs within **1**, **3**, and **4**. Following charge separation at 295 K, we observed an intense spin-polarized RP signal (Figure 5). The spectra were fit with the model developed by Till and Hore,[65] using the hyperfine coupling constants calculated by DFT for ($DMJ^{+\bullet}$−An) and measured by EPR for $NI^{-\bullet}$ (see Supporting Information). The 2*J* values obtained from the fits are presented in Table 1. The 2*J* value for **2** was determined directly from magnetic field effects (MFEs) on the ^{3*}An yield formed upon charge recombination because 2*J* for **2** is too large to be measured accurately using the spin-polarized RP signal obtained by TREPR.

Transport Calculations. The electronic transmission through the thiol-substituted bridges shows a considerable difference in the magnitude of the transmission between **2S** and **4S** and the much lower **1S** and **3S** (Figure 6). The relationship between **1S** and **3S** is more involved, with **1S** lower over a limited energy range near the Fermi energy and **3S** lower as the system approaches the resonances.

The energy of the isolated molecules as a function of the dihedral angle was calculated in order to determine how much conformational flexibility is energetically feasible (Figure 7). The dihedral angle was varied from 0° to 90° for the cases of **1S**, **2S**, and **3S** and from 0° to 10° in the case of **4S**. Changing the dihedral angle in **4S** stretches the C−O−C bonds that tether the rings, and consequently the structure is much more restricted. The dihedral angles that are energetically allowed tend to vary only 5−10° from *kT* at room temperature, suggesting that the dihedral angle is not changing significantly.

The transmission through the thiol-substituted bridges as a function of dihedral angle was calculated in order to determine how the change in dihedral angle affects the transmission (Figure 8). The linearly conjugated system **2S** shows the largest dependence on dihedral angle, while **3S** and **4S** show the least dependence on dihedral angle. However, the dihedral angle of **4S** cannot be greatly varied due to the tethering of the rings, as mentioned previously. The cross-conjugated system, **1S**, never approaches the high transmission of **2S** even when the dihedral approaches 0°.

Discussion

The photoinduced charge transfer dynamics of **1**−**4** are highly dependent on the bridge conjugation. Charge transfer through the cross-conjugated 1,1-diphenylethene bridge in **1** is nearly 30 times slower than through its linearly conjugated *trans*-stilbene counterpart in **2**. According to the transmission spectra, interference in cross-conjugated molecules suppresses π system transport, thereby revealing the much slower σ system transport. Therefore, it is expected that **1** should have a rate similar to a D−B−A system that uses a σ-system bridge, such as compound **3**. This holds true, as τ_{CS} is slightly faster in **1** versus **3**. This slight increase in rate for **1** could be due to multiple factors such as either inelastic transport or the partial π conjugation that exists in cross-conjugation. This is counterbalanced somewhat by direct $\pi-\pi$ overlap between the phenyls in diphenylmethane. However, what is most important is the similarity in τ_{CS} for **1** and **3**, which strongly suggests that the σ system is the primary transfer pathway through the cross-conjugated bridge in **1**.

Bridge **4** provides another example of a cross-conjugated bridge; however, the cross-conjugated component is a ketone rather than an ethylene group. The transmission curve of **4** strongly implies that the CS and CR times should be faster than **1**, and more like that of a linearly conjugated molecule. This is borne out by the data which show that both τ_{CS} and τ_{CR} are similar for **2** and **4**. This result may seem counterintuitive, but previous transmission curve calculations have shown that having an electron-withdrawing substituent directly bonded to the double bond shifts the energy of the interference feature and hence changes the conductance significantly.[66,67]

The charge recombination rates do not follow the same trend observed for charge separation. In order to better understand this difference, the magnitude of the magnetic spin−spin exchange interaction, 2*J*, was obtained using either TREPR spectroscopy on the RPs or MFE measurements on the yield of ^{3*}An resulting from CR, both of which have been described previously.[65,68] As mentioned above, the electronic coupling, V_{DA}, gives the effective interaction energy between the donor

(65) Till, U.; Hore, P. J. *Mol. Phys.* **1997**, *90*, 289–296.
(66) Solomon, G. C.; Andrews, D. Q.; Van Duyne, R. R.; Ratner, M. A. *ChemPhysChem* **2009**, *10*, 257–264.
(67) Andrews, D. Q.; Solomon, G. C.; Van Duyne, R. P.; Ratner, M. A. *J. Am. Chem. Soc.* **2008**, *130*, 17309–17319.
(68) Scott, A. M.; Miura, T.; Ricks, A. B.; Dance, Z. E. X.; Giacobbe, E. M.; Colvin, M. T.; Wasielewski, M. R. *J. Am. Chem. Soc.* **2009**, *131*, 17655–17666.

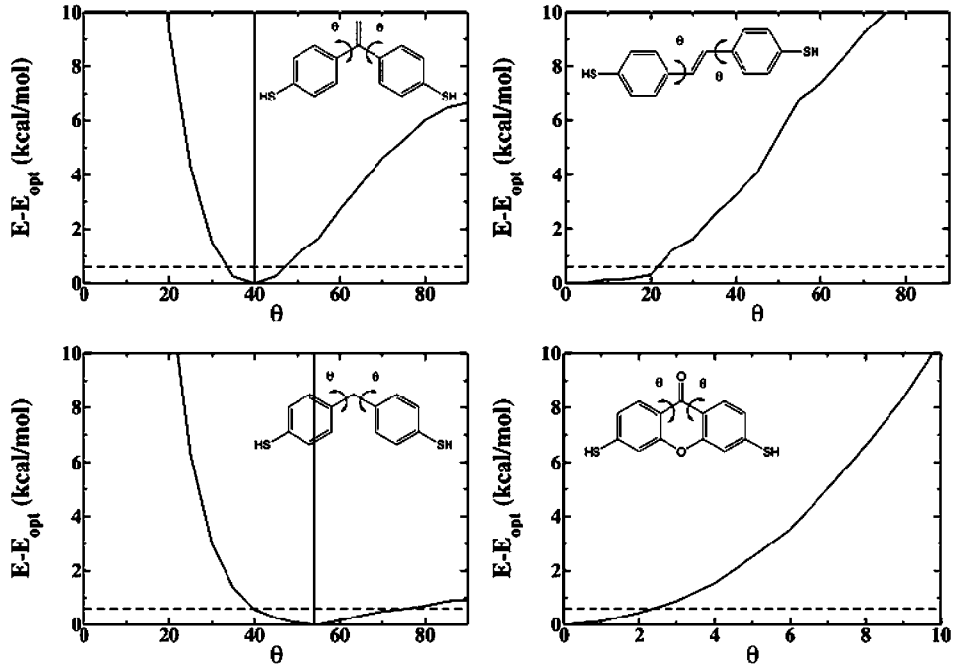

Figure 7. The energy of the thiol-substituted bridges, above the geometrically optimized structures, as a function of the dihedral between the phenyl rings and the bridging unit. In each case the dashed horizontal line indicates *kT* at room temperature and a vertical line indicates the dihedral in the optimized structures. In the case of **4S** only a very limited range is shown, as this dihedral change is stretching the C−O−C bonds tethering the rings together.

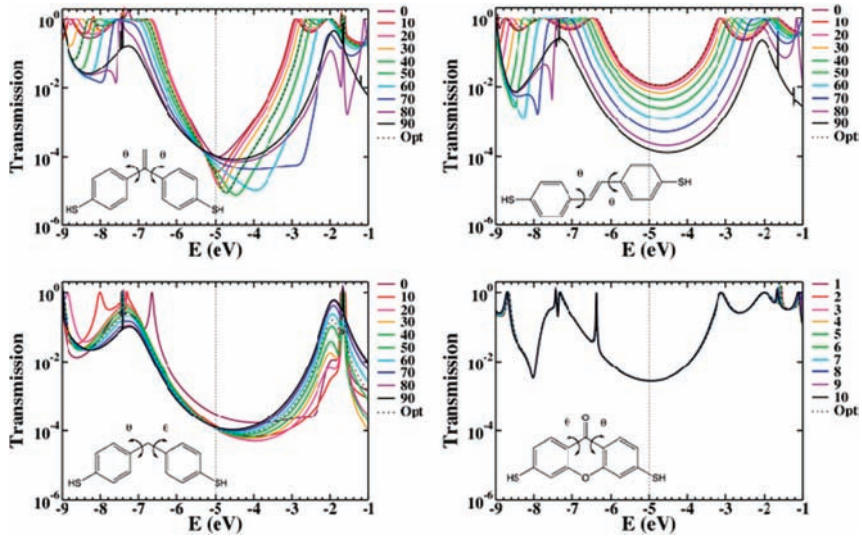

Figure 8. The transmission through the thiol-substituted bridges at a range of dihedral angles, showing the extent to which the electronic coupling is perturbed by any of this kind of conformational flexibility in the systems. The dashed vertical line indicates the Fermi energy in the calculations.

and acceptor, which will influence the charge separation and recombination rates. Since $2J \propto V_{DA}^2$ and depends on orbital overlap,[69,70] variations in 2*J* yield information on the dependence of V_{DA} on bridge structure. Since the bridges in **1**−**4** have some torsional flexibility about their single bonds, their equilibrium geometries pre- and postcharge separation may be different. Since orbital overlap depends on this geometry, it is likely that V_{DA} for charge separation and recombination are different. As 2*J* is only measured for the CR reaction, it only yields information related to CR, and not CS. It is common for the CR lifetimes to increase as 2*J* decreases, which is the trend observed in this series. Molecule **1** has the smallest 2*J* value and has the longest CR time, and consequently we expect V_{DA} to be the smallest for **1**. In contrast, molecule **2** has the largest 2*J* value and the shortest CR time, and we expect V_{DA} to be large, as the bridge is fully linearly conjugated. While the CR lifetime trend does not follow that of the CS lifetimes, it does follow what is expected based on 2*J* values.

The results from the electron transport calculations show energy regions where the trends observed in the CS and CR times are reflected in the magnitude of the transmission; but any sort of quantitative agreement is poor. Above the Fermi energy, but below the energy at which the resonant transport peaks occur, in the range of −3.5 to −4.0 eV, the trends

(69) Kobori, Y.; Sekiguchi, S.; Akiyama, K.; Tero-Kubota, S. *J. Phys. Chem. A* **1999**, *103*, 5416–5424.
(70) Paddon-Row, M. N.; Shephard, M. J. *J. Phys. Chem. A* **2002**, *106*, 2935–2944.

observed in the CS rates are somewhat evident. In this region, **1S** and **3S** have much lower transmission than **2S** and **4S**, although the transmission through **4S** never exceeds **2S** in these calculations. Closer to the Fermi energy, in the range between −5.5 and −4.5 eV, the transmission through **1S** drops significantly and the trends in the rates of CR are reflected in the transmission.

Bridges **1**, **2**, and **3** have more rotational freedom than bridge **4**. This is of concern, as the calculated electronic transmission curves (Figure 6) neglect the role that conformational fluctuations can have in changing the coupling through a molecule by only taking into account the minimum energy structures for the bridges. Further, in addition to the topological differences in the bonding between **1** and **2**, there are also significant differences in the planarity of the molecules, which is a factor that has direct bearing on the electronic coupling in conjugated systems.[71,72] The effects of twisting in the structure, as well as a sense of the conformational flexibility at room temperature, was assessed by examining the bridges as the dihedral angle between the phenyl rings and the central component of the bridge is varied. As expected, there is very little conformational flexibility in **4S** compared with the other structures, while **3S** showed the greatest range of accessible motion.

Conformational flexibility influences electron transfer and transport rates by modulating the electronic coupling through the system. The transmission through the thiol-substituted bridges as a function of dihedral angle was also determined (Figure 8). The combination of these two results gives insight into one aspect that is expected to lead to a lack of agreement between the calculations and measured rates. The linearly conjugated system **2S** shows the largest dependence on dihedral angle, which is expected for a system where the π-system dominates the transport. Any deviation from the optimal planar structure results in a decrease in the transmission and therefore the conductance. This increased flexibility may contribute to the fact that the observed CS rate is faster in **4** than in **2**, whereas there is higher calculated transmission through **2S** compared with **4S** across a large energy range.

While **1S** and **3S** both have a reasonable degree of conformational flexibility, the variation in the transmission with dihedral angle change is not unidirectional. Above the Fermi energy, the transmission through **1S** increases with decreasing dihedral angle and decreases with increasing dihedral angle, whereas in **3S** the behavior is reversed. The differences in these two cases arise as the decreasing dihedral angle shifts the proximate resonance closer to the Fermi energy in the case of **1S**, whereas it decreases the magnitude of the resonant transmission in **3S**. In both cases, however, the conformationally averaged transmission would not be expected to shift so far from the minimum energy value as it would in **2S**. It is also interesting to note that while **3S** has the largest conformational flexibility, this does not result in a significant change in the transport, as the σ system mediates transport through the saturated central part of the bridge and is significantly less sensitive to conformational changes.

(71) Woitellier, S.; Launay, J. P.; Joachim, C. *Chem. Phys.* **1989**, *131*, 481–488.
(72) Venkataraman, L.; Klare, J. E.; Nuckolls, C.; Hybertsen, M. S.; Steigerwald, M. L. *Nature* **2006**, *442*, 904–907.

Conclusions

We have prepared a series of molecules to test the effect of cross-conjugated bridges on charge transfer in D−B−A systems. We found that charge transfer through a cross-conjugated 1,1-diphenylethene bridge occurs about 30 times slower through its linearly conjugated counterpart *trans*-stilbene. Comparisons of the charge transfer rates obtained for the 1,1-diphenylethene bridge with that of a diphenylmethane bridge shows that the former most likely uses its σ system as its primary charge transfer pathway. The data obtained for the cross-conjugated xanthone bridge illustrates how substituent effects can shift the energy of the cross-conjugation antiresonance and thereby control the electron transfer rate through the bridge. Computations allow us to qualitatively compare electron transport theory with electron transfer experiments. From these results we were able to observe the trends in conductance through bridges **1S**−**4S** reflected in the charge transfer rates through bridges **1**−**4**. Long RP lifetimes are often the goal of research on D−B−A molecules, but the synthesis of long bridges generally involves many steps to make molecules having long RP lifetimes. Our results show that changing the electronic coupling of the bridge can change the electron transfer rates dramatically so that much simpler molecules can be used to prolong RP lifetimes.

Acknowledgment. This work was supported by the Chemical Sciences, Geosciences, and Biosciences Division, Office of Basic Energy Sciences, DOE under grant no. DE-FG02-99ER14999 (M.R.W.). M.A.R. thanks the NSF Chemistry Division. M.T.C. thanks the Link Foundation for a fellowship. We thank Mr. Thomas Michl for assistance in synthesizing compound **1**.

Supporting Information Available: Details regarding the synthesis and characterization of **1**−**4**, additional transient absorption data, and complete ref 53. This material is available free of charge via the Internet at http://pubs.acs.org.

JA107420A